Dependence of crystal orientation in Al-induced crystallized poly-Si layers on Si02 insertion layer thickness

著者別名	都甲 薫, 末益 崇
journal or publication title	Journal of crystal growth
volume	356
page range	65-69
year	2012-10
権利	(C) 2012 Elsevier B.V. NOTICE: this is the author's version of a work that was accepted for publication in Journal of crystal growth. Changes resulting from the publishing process, such as peer review, editing, corrections, structural formatting, and other quality control mechanisms may not be reflected in this document. Changes may have been made to this work since it was submitted for publication. A definitive version was subsequently published in PUBLICATION, Volume 356, 2012, DOI:10.1016/j.jcrysgro.2012.07.015
URL	http://hdl.handle.net/2241/117630

doi: 10.1016/j.jcrysgro.2012.07.015

Dependence of crystal orientation in Al-induced crystallized poly-Si layers on SiO_2 insertion layer thickness

Atsushi Okada[a], Kaoru Toko[a], Kosuke O. Hara[b], Noritaka Usami[b,c], and Takashi Suemasu[a,b]

[a]*Institute of Applied Physics, University of Tsukuba, 1-1-1 Tennodai, Tsukuba, Ibaraki 305-8573, Japan*

[b]*Japan Science and Technology Agency, CREST, 5, Sanbancho, Chiyoda-ku, Tokyo 102-0075, Japan*

[c]*Institute for Materials Research, Tohoku University, 2-1-1, Katahira, Aoba-ku, Miyagi 980-8577, Japan*

We have fabricated poly-Si thin films on fused silica substrates by the Al-induced crystallization (AIC) method with SiO_2 insertion layers of various thicknesses (0-20 nm). The growth morphologies of poly-Si layers were dramatically changed by the SiO_2 thickness, *i.e.*, thin layers (2 nm) provided high growth rates and (100) orientations, and thick layers (10 nm) provided low growth rates and (111) orientations. These results showed that the crystal orientation of AIC-Si significantly depends on the diffusion rate of Si atoms into the Al layer.

PACS: 61.05.cp; 61.05.jh; 68.55.ag

Keywords: A1. Growth models; A3. Solid phase epitaxy; B2. Semiconducting silicon; B3. Solar cells

1. Introduction

The Al-induced crystallization (AIC) method is known as a method for obtaining thin poly-Si layers on glass substrates, where amorphous Si (a-Si) layers on Al are transformed into a crystalline phase via exchange between the Al and Si layers during annealing [1]. This method enables us to fabricate seed layers for epitaxially grown absorbers for thin-film solar cells on inexpensive SiO_2 substrates [2-7]. Conventional solid phase crystallization (SPC) requires temperatures higher than 600°C, and the Si grains obtained are as small as a few μm [8]. In the AIC method, Si crystallizes at relativity low temperatures in the range of 400-500°C, and large grains of tens of μm in size can be obtained even on non-lattice-matched substrates [9,10]. Therefore, the Si seed crystals fabricated by the AIC method seem to enable the growth of high-quality devices such as thin-film solar cells and thin-film transistors on low-cost glass substrates [11-15]. The crystal orientation is critical for device performances [16]. Thus, the control of crystal orientations in the poly-Si layers is required.

However, factors determining the preferential crystal orientation of AIC-Si layers remain an open question. Preferential (100) orientation of the AIC-Si layers has been reported [9,13,17]. On the other hand, growth of (111)-oriented Si layers has been also reported [15,18]. Kurosawa *et al.* showed that the preferential orientation of AIC-Si on fused silica can be controlled by changing the exposure time of Al in air, and they proposed

a model showing that the orientation of AIC-Si is determined by the crystal phase of the native Al oxide [19]. In contrast, Jung *et al*. considered that the preferential orientation depends on the annealing temperature, and proposed a model showing that the growth rate of AIC-Si determines the preferential orientation [20]. In this study, our aim was to investigate the influence of Si diffusion rate on the preferential orientation of AIC-Si. We also aimed to develop a method to control the crystal orientation of AIC-Si. For this purpose, we introduced SiO_2 layers with various thicknesses as intermediate layers between the a-Si and Al layers and carried out the AIC method. The SiO_2 layer thickness is easier to control compared to the thickness of a native Al oxide. In addition, the effect of the intermediate layer crystallinity on the AIC-Si is negligible when we discuss the crystal orientation of AIC-Si layers.

2. Experimental procedures

Fused silica wafers were used as substrates in this work. A 100-nm-thick Al film was sputtered at room temperature (RT) on the substrate. Next, an amorphous SiO_2 layer was subsequently sputtered at RT on the Al layer, followed by sputtering a 100-nm-thick a-Si film at RT without breaking the vacuum. The thickness of the SiO_2 layer was varied from 0 to 20 nm. All the depositions were carried out by radio-frequency (RF) magnetron sputtering. For comparison, conventional AIC method was also performed, that is,

deposition of Al layers, followed by breaking the vacuum to form a native Al layer for 48 h, and the subsequent deposition of a-Si layers. The argon pressure during the sputtering was 0.2 Pa. The RF power was set at 100 W. The AIC method was carried out by annealing the samples in N_2 atmosphere at 500 °C for 10 h. Sample preparation was summarized in Table 1. The surface morphologies of some of the samples were observed during annealing by optical microscopy. After annealing, the Al and oxide layers were etched away using a HF solution (HF: 2%). The crystal orientation of AIC-Si was characterized by electron backscatter diffraction (EBSD) measurement.

3. Results and discussion

The time evolution of optical microscope images for sample D, prepared with a 2-nm-thick SiO_2 intermediate layer, is shown in Figs. 1(b)-1(e), and those for sample H, prepared with a 10-nm-thick SiO_2 layer, are shown in Figs. 1(f)-1(i). Figure 1(a) shows the expected schematic cross-sectional diagram of each crystallization stage. Upon heating, interdiffusion of Al and Si atoms begins. After the diffused atoms become supersaturated, they begin to nucleate. The time necessary for Si nuclei to be observed with an optical microscope is defined as the incubation time. After that, these nuclei were grown laterally. The change of Si crystal radius per unit time is defined as growth rate. In growth stage, few nuclei were generated. The dependence of the incubation time and growth rate on the

thickness of the SiO_2 intermediate layer is shown in Fig. 2. The results for sample I were excluded as described later. This graph shows that the thicker the SiO_2 intermediate layer, the longer the incubation time and the smaller the growth rate. This means that the SiO_2 intermediate layer works as a diffusion barrier for Si atoms, which is supported by the fact that the diffusion coefficient of Si in SiO_2 is approximately 1000 times smaller than that in Al [21,22]. On the basis of the results shown in Fig. 2, it can safely be stated that the diffusion rate of Si depends on the SiO_2 intermediate layer thickness.

Figure 3 shows the crystal orientation mappings obtained by EBSD for AIC-Si layers fabricated with various SiO_2 intermediate layer thicknesses. When we employed the conventional AIC method, highly (111)-oriented AIC-Si layers were formed in sample A as shown in Fig. 3(a). We next discuss the influence of SiO_2 intermediate layer thickness on the AIC-Si crystal orientation. As shown in Figs. 3(b) and 3(f), the grain size of AIC-Si is considerably small, less than 1 μm both when the SiO_2 intermediate layer thickness is zero (sample B) and when it is very thick (20 nm, sample I). In the case of AIC-Si formed without the SiO_2 layer as in sample B, the Si atoms were thought to diffuse into the Al layer very rapidly, causing supersaturation shortly upon heating, and thus the Si atoms started to nucleate everywhere at the Si/Al interface, resulting in small grains as shown in Fig 3(b). In the case of very thick SiO_2 layer (20 nm, sample I), the results have not been completely understood. In general, sputtered SiO_2 films contain a certain amounts of

defects [23]. We speculate that these defects might significantly influence the diffusion of Si atoms and thereby generation of Si nuclei at the Al/SiO_2 interface, making it difficult to understand the AIC process by the simple model shown in Fig. 1. In contrast, when the SiO_2 intermediate layer was 2-10 nm in thickness (samples C-H), the AIC-Si grains exceeded tens of μm in size as shown in Figs. 3(c)-3(e). We think that the Si diffusion was suppressed moderately by this SiO_2 layer, and thus only a small number of Si nuclei were generated at the Al/SiO_2 interface, leading to lateral growth of Si nuclei as shown in Figs. 3(c)-3(e). Figure 4 shows the SiO_2 intermediate layer thickness dependence of crystal orientation fractions of Si. The results obtained for sample I were not included. When the SiO_2 intermediate layer was 1 nm thick, the AIC-Si became highly (100) oriented. On the other hand, highly (111)-oriented AIC-Si layers were formed when the SiO_2 intermediate layer was 10 nm thick. The crystal orientation was determined from grains whose misorientation from the ideal (100) and (111) planes was less than 10°. The areas other than the (100) and (111) planes were much smaller, and thus were excluded in Fig. 4. These results suggest that the orientation of a poly-Si thin film fabricated by the AIC method depends significantly on the SiO_2 layer thickness, thereby the diffusion rate of Si.

Next, we discuss the mechanism of preferential AIC-Si crystal orientation dependence on the SiO_2 intermediate layer thickness, and thus the diffusion rate of Si atoms to the Al layer. The surface energy in crystalline Si is the lowest for the (111) plane, followed by the

(100) plane [24]. We think that the crystal plane dependence of the interface energy at the crystalline Si/amorphous SiO_2 interface is mostly the same as that in the crystalline Si, because SiO_2 has no anisotropy. The growth rate in Si is the largest on the (100) plane [25]. The nucleation of Si occurs at the Al/SiO_2 interface in AIC, because the concentration of Si is the largest there within the Al layer. When the SiO_2 intermediate layer is thick and the Si diffusion rate is small, the concentration of Si in the Al increases gradually. Therefore, in the nucleation stage, only the most stable nuclei, (111)-oriented Si nuclei, are generated. In the crystal growth stage, these (111)-oriented nuclei grow laterally. As a result, the poly-Si film becomes (111) oriented. This (111) domination appears to contradict the theory presented by Schneider *et al* [26]. This contradict is possibly originated from the difference in the Al and Si thicknesses, because these thicknesses significantly affect the orientation of the AIC-Si layer [27]. In contrast, when the SiO_2 intermediate layer is thin and the Si diffusion rate is large, the degree of supersaturation is likely to become large. Therefore, in the nucleation stage, (100)-oriented nuclei, the second most stable nuclei, are generated in addition to the (111)-oriented nuclei. In the crystal growth stage, (100)-oriented nuclei grow rapidly because these grains have (100) facets. Therefore, (100)-oriented nuclei finally become dominant.

4. Conclusions

In summary, we have fabricated poly-Si thin films on fused silica substrates by the AIC method using SiO_2 intermediate layers with various thicknesses (0-20 nm) between the a-Si (100 nm) and Al (100 nm) layers. The incubation time and growth rate of the Si grains depended on the SiO_2 layer thickness. With increasing SiO_2 layer thickness from 2 to 10 nm, the crystal orientation of the AIC-Si changed gradually from the (100) to (111) orientation. This selective formation technique of (100) and (111) oriented poly-Si films opens up a possibility of high-quality epitaxial templates for thin film devices.

Acknowledgments

This work was financially supported by Japan Science and Technology Agency, CREST and Grant-in-Aid for Research Activity Start-up (No. 23860011 MEXT). A part of this work was conducted by the AIST Nano-Processing Facility, supported by "Nanotechnology Network Japan" of MEXT, Japan.

References

[1] O. Nast, T. Puzzer, L. M. Koschier, A. B. Sproul, and S. R. Wenham, Appl. Phys. Lett. 73 (1998) 3214.

[2] Z. Shi and M. A. Green, Prog. Photovoltaics 6 (1998) 247.

[3] P. I. Widenborg and A. G. Aberle, J. Cryst. Growth 242 (2002) 270.

[4] E. Pihan, A. Slaoui, and C. Maurice, J. Cryst. Growth 305 (2007) 88.

[5] H. Kuraseko, N. Orita, H. Koaizawa, and M. Kondo, Appl. Phys. Express 2 (2009) 015501.

[6] I. Gordon, L. Carnel, D. Van Gestel, G. Beaucarne, and J. Poortmans, Thin Solid Films 516 (2008) 6984.

[7] B. R. Wu, S. Y. Lo, D. S. Wuu, S. L. Ou, H. Y. Mao, J. H. Wang, and R. H. Horng, Thin Solid Films 520 (2012) 5860.

[8] R.B. Bergmann, G. Oswald, M. Albrecht, and V. Gross, Sol. Energy Mater. Sol. Cells 46 (1997) 147.

[9] H. Kim, D. Kim, G. Lee, D. Kim, and S. H. Lee, Sol. Energy Mater. Sol. Cells 74 (2002) 323.

[10] S. Gall, M. Muske, I. Sieber, O. Nast, and W. Fuhs, J. Non-Cryst. Solids 299-302 (2002) 741.

[11] Y. Ishikawa, A. Nakamura, Y. Uraoka, and T. Fuyuki, Jpn. J. Appl. Phys. 43 (2004) 877.

[12] I. Gordon, L. Carnel, D. Gestel, G. Beaucarne, and J. Poortmans, Prog. Photovoltaic 15 (2007) 575.

[13] P. Prathap, O. Tuzun, D. Madi, and A. Slaoui, Sol. Energy Mater. Sol. Cells 95 (2011) S44.

[14] K. Toko, M. Kurosawa, H. Yokoyama, N. Kawabata, T. Sakane, Y. Ohta, T. Tanaka, T. Sadoh, and M. Miyao, Appl. Phys. Express 3 (2010) 075603.

[15] D. Tsukada, Y. Matsumoto, R. Sasaki, M. Takeishi, T. Saito, N. Usami, and T. Suemasu, Appl. Phys. Express 2 (2009) 051601.

[16] S. M. Sze, Physics of Semiconductor Devices, p. 386, 2nd ed. (Wiley, New York, 1981)

[17] S. Gall, J. Schneider, J. Klein, K. Hübener, M. Muske, B. Rau, E. Conrad, I. Sieber, K. Petter, K. Lips, M. Stöger-Pollach, P. Schattschneider, and W. Fuhs, Thin Solid Films 511-512 (2006) 7.

[18] Y. Sugimoto, N. Takata, T. Hirota, K. Ikeda, F. Yoshida, H. Nakashima, and H. Nakashima, Jpn. J. Appl. Phys. 44 (2005) 4770.

[19] M. Kurosawa, N. Kawabata, T. Sadoh, and M. Miyao, Appl. Phys. Lett. 95 (2009) 132103.

[20] M. Jung, A. Okada, T. Saito, T. Suemasu, and N. Usami, Appl. Phys. Express 3 (2010) 095803.

[21] S. Fujikawa, K. Hirano, and Y. Fukushima, Metall. Trans. A 9A (1978) 1811.

193 [22] S. Fukatsu, T. Takahashi, and K. M. Itoh, Appl. Phys. Lett. 83 (2003) 3897.

194 [23] Y. Urabe, T. Sameshima, K. Motai, and K. Ichimura, Jpn. J. Appl. Phys. 47 (2008) 8003.

195 [24] A. A. Stekolnikov, J. Furthmuller, and F. Bechstedt, Phys. Pev. B 65 (2002) 115318.

196 [25] L. Csepregi, E. F. Kennedy, and J. W. Mayer, J. Appl. Phys. 49 (1978) 3906.

197 [26] J. Schneider, A. Sarikov, J. Klein, M. Muske, I. Sieber, T. Quinn, H.S. Reehal, S. Gall,

198 and W. Fuhs, J. Crystal Growth 287 (2006) 423.

199 [27] M. Kurosawa, K. Toko, N. Kawabata, T. Sadoh, and M. Miyao, Solid-State Electron. 60

200 (2011) 7.

201

Fig. 1 (a) Schematic cross-sectional diagrams of each crystallization stage, optical micrographs of surface morphologies of sample D, prepared with a 2-nm-thick SiO_2 intermediate layer, after annealing for (b) 40, (c) 50, (d) 55, and (e) 60 min, and those for sample H, prepared with a 10-nm-thick SiO_2 intermediate layer after annealing for (f) 120, (g) 150, (h) 180, and (i) 210 min.

Fig. 2 Dependence of the incubation time and growth rate on the SiO_2 intermediate layer thickness.

Fig. 3 Dependence of crystal orientation mappings of AIC-Si on the SiO_2 intermediate layer thickness for (a) sample A (native Al-oxide), (b) sample B (0 nm), (c) sample D (2 nm), (d) sample G (5 nm), (e) sample H (10 nm), and (f) sample I (20 nm).

Fig. 4 Dependence of AIC-Si crystal orientation fractions on the SiO_2 intermediate layer thickness.

Table 1 Preparation of samples A-I. Al layer thickness, air exposure time, SiO_2 and a-Si layer thicknesses are shown.

Sample	Al (nm)	Air exposure (h)	SiO_2 (nm)	Si (nm)
A	100	48	0	100
B	100	0	0	100
C	100	0	1	100
D	100	0	2	100
E	100	0	3	100
F	100	0	4	100
G	100	0	5	100
H	100	0	10	100
I	100	0	20	100

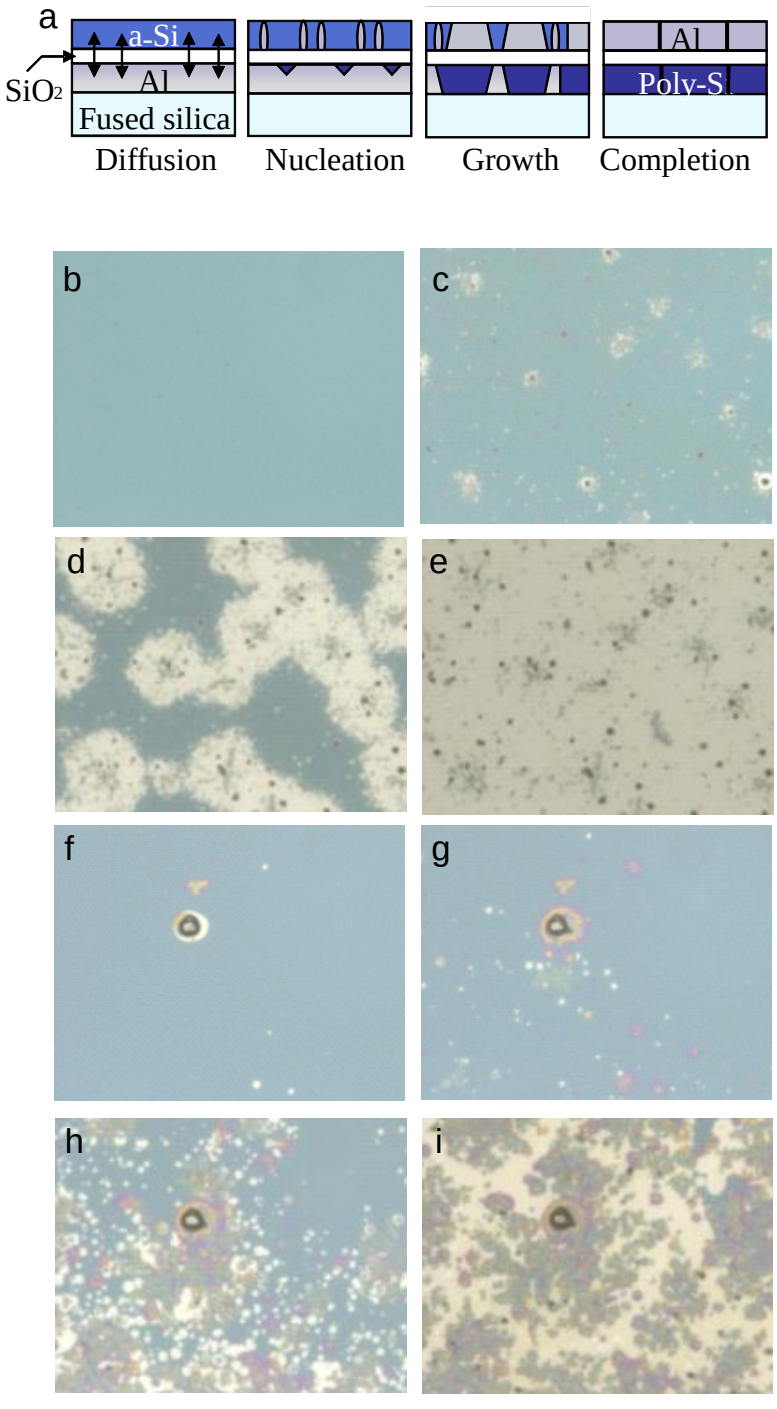
a
a-Si
Al
SiO2
Fused silica
Diffusion
Nucleation
Growth
Al
Poly-Si
Completion
b
c
d
e
f
g
h
i
50 μm

Figure 1

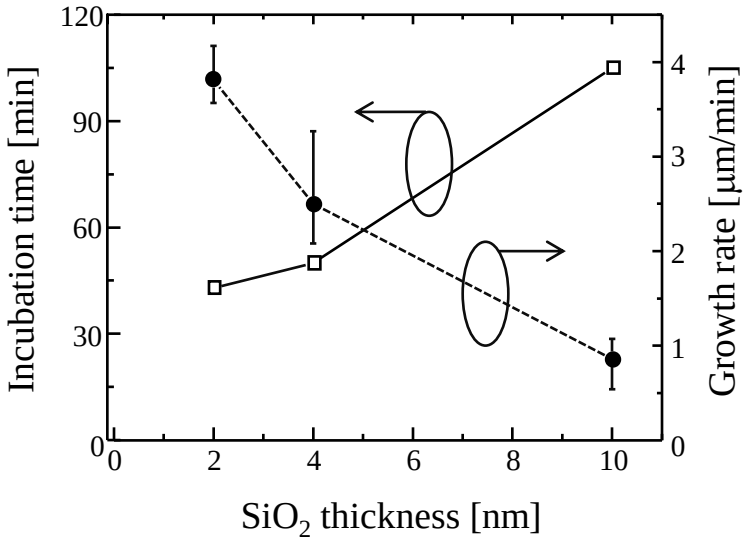
120
90
60
30
0
Incubation time [min]
0
2
4
6
8
10
SiO2 thickness [nm]
4
3
2
1
0
Growth rate [μm/min]

Figure 2

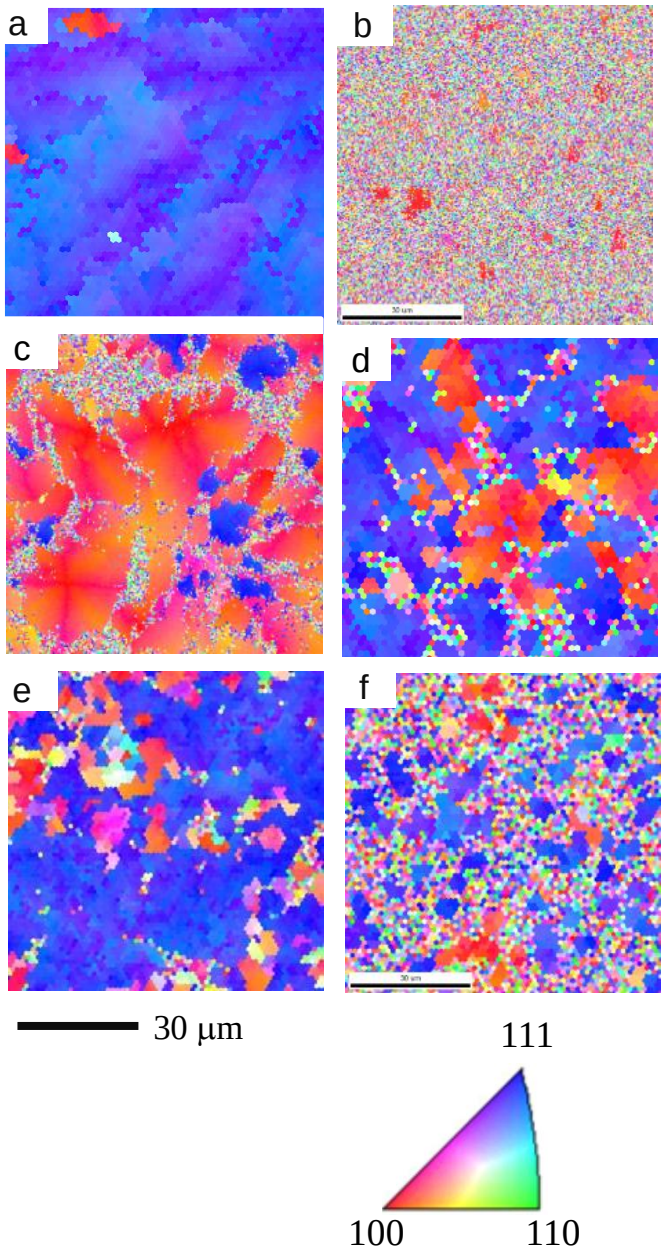

Figure 3

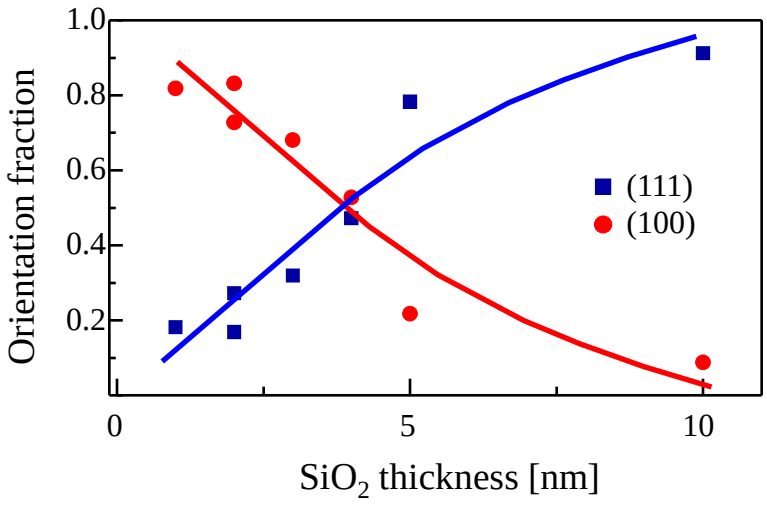
1.0
0.8
0.6
0.4
0.2
Orientation fraction
0
5
10
SiO2 thickness [nm]
(111)
(100)

Figure 4